ARTICLES

Charge Separation and Recombination in Photoexcited Oligo(*p*-phenylene vinylene): Perylene Bisimide Arrays Close to the Marcus Inverted Region

Edwin H. A. Beckers,[†] Stefan C. J. Meskers,[†] Albertus P. H. J. Schenning,[†] Zhijian Chen,[‡] Frank Würthner,*[,‡] and René A. J. Janssen*[,†]

Laboratory of Macromolecular and Organic Chemistry, Eindhoven University of Technology, P.O. Box 513, 5600 MB Eindhoven, The Netherlands, and Institut für Organische Chemie, Universität Würzburg, Am Hubland, D-97074 Würzburg, Germany

Received: March 6, 2004

The kinetics of photoinduced intramolecular charge separation and subsequent charge recombination of three oligo(*p*-phenylene vinylene)-perylene bisimide-oligo(*p*-phenylene vinylene) arrays has been studied using femtosecond pump−probe spectroscopy in solvents of different polarity. The reduction potentials of three donor−acceptor−donor molecules differ strongly as a consequence of the four substituents (R = 4-*tert*-butylphenoxy, H, or Cl) at the bay position of the central perylene bisimide unit. The experiments indicate that charge separation in these molecules occurs from the first excited singlet state of the perylene bisimide moiety to the charge-separated state (CSS) and to the lowest electronically excited state level of the charge-separated state (CSS*). For R = H and Cl, the rates for charge separation and charge recombination decrease with increasing change in the Gibbs free energy, and hence the molecules represent an exceptional example of molecules in which both charge separation and recombination occur close to or in the Marcus inverted region.

Introduction

The kinetics of photoinduced charge separation reactions in π-conjugated donor−acceptor systems is important to natural and artificial light energy conversion.[1] Marcus theory for electron transfer predicts that this reaction can occur in different regions, depending on the relative magnitude of the change in Gibbs free energy ($-\Delta G_0$) and the reorganization energy (λ).[2] In the "normal region" ($-\Delta G_0 < \lambda$), the rate constant increases with increasing driving force ($-\Delta G_0$), whereas in the "inverted region" ($-\Delta G_0 > \lambda$), the rate constant should decrease with increasing $-\Delta G_0$. This prediction of Marcus theory has attracted considerable interest and was experimentally first verified by Closs and Miller 20 years ago.[3] Presently, numerous examples of inverted region behavior have been reported for charge recombination, but it remains quite elusive in photoinduced charge separation.[4] One exception is the recent work of Mataga et al., who elegantly demonstrated inverted region behavior in charge separation in porphyrin-imide dyads, utilizing the higher-energy S_2 state to increase $-\Delta G_0$.[5]

Here, we describe the photoinduced electron transfer and recombination kinetics of three oligo(*p*-phenylene vinylene)-perylene bisimide-oligo(*p*-phenylene vinylene) (OPV-PERY-OPV) arrays (**1**−**3**, Figure 1) and demonstrate that for **2** and **3** both forward and backward electron transfer occur in the inverted region. These donor−acceptor−donor arrays differ only by the substituents at the bay positions of the central PERY moiety. The substituents *tert*-butylphenoxy, hydrogen, and chlorine were chosen to create an increasing reduction potential of the perylene bismide and thereby an increase of $-\Delta G_0$.

Results and Discussion

Compound **2** has been described previously.[6] Compounds **1** and **3** were synthesized by reacting (*E*,*E*,*E*)-4-[4-{4-(3,4,5-tridodecyloxystyryl)-2,5-bis[(*S*)-2-methylbutoxy]styryl}-2,5-bis[(*S*)-2-methylbutoxy]styryl]aniline[6] with the appropriately substituted 3,4:9,10-perylenetetracarboxylic dianhydrides in the presence of zinc acetate in quinoline at 190 °C (Figure 1). Compounds **1** and **3** were fully characterized using NMR spectroscopy and mass spectrometry. The UV/vis absorption spectra of **1**−**3** are shown in Figure 2. The spectra exhibit the characteristic $\pi-\pi^*$ absorption of the OPV unit at ∼435 nm for each triad. The absorptions at higher wavelength are the vibronically resolved transitions of the perylene bisimide chromophores. Going from **1** to **3**, there is a continuous shift of this band to higher energy, and accordingly, the energy of the lowest singlet excited state increases (E_{00} = 2.13, 2.32, and 2.38 eV for **1**−**3**, respectively when recorded in CH_2Cl_2).

Each of the three triads **1**−**3** exhibits a reversible oxidation wave in the cyclic voltammogram. The first oxidation potentials of **1**−**3** are very similar (E_{ox} = +0.34, +0.31, and +0.33 V vs Fc/Fc^+ in CH_2Cl_2, respectively). The reduction potentials vary much more (E_{red} = −1.17, −1.02, and −0.80 V) and reflect the difference in the electron donating and accepting character of the substituents on the perylene bisimide moiety.

* Corresponding authors. E-mail: wuerthner@chemie.uni-wuerzburg.de; r.a.j.janssen@tue.nl.
† Eindhoven University of Technology.
‡ Universität Würzburg.

10.1021/jp048980n CCC: $27.50
Published on Web 08/03/2004

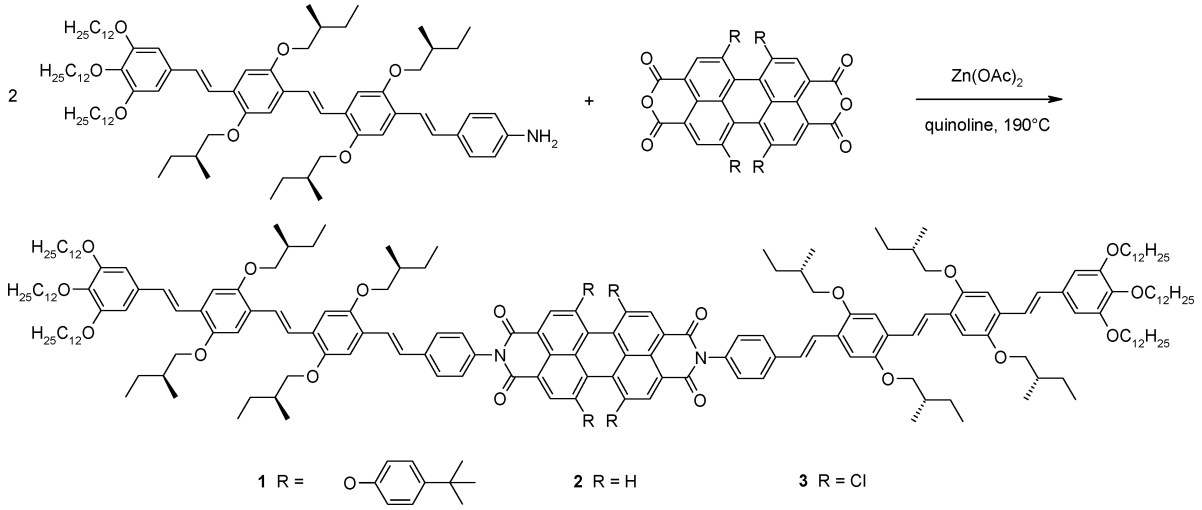

Figure 1. Synthesis and structures of the three donor−acceptor−donor arrays **1**−**3**.

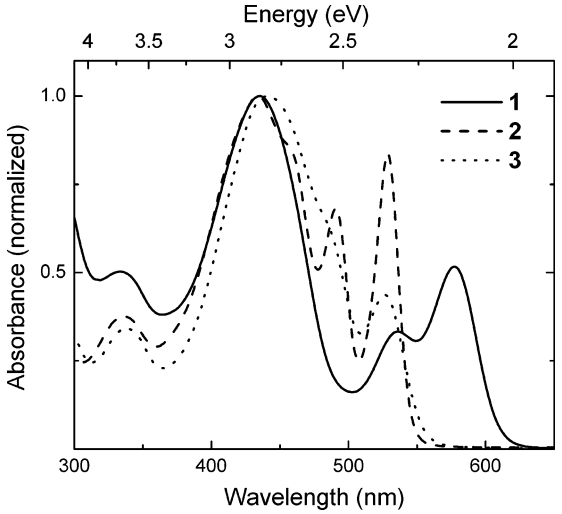

Figure 2. Normalized UV/vis absorption spectra of compounds **1**−**3**.

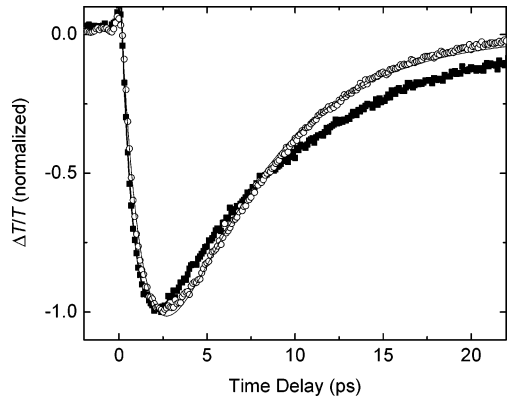

Figure 3. Normalized differential transmission dynamics of **3** in $CHCl_3$ ($\epsilon_s = 4.81$, closed squares) and benzonitrile ($\epsilon_s = 25.3$, open circles) recorded at (1450 nm) with excitation at 450 nm, together with a biexponential fit to the data (solid lines).

The rates for charge separation (k_{CS}) and recombination (k_{CR}) were determined for **1**−**3** in six solvents with varying polarity ($\epsilon_s = 2.38-25.3$) by monitoring the transient absorption of the $OPV^{+\bullet}$ radical cation at 1450 nm[6] after excitation of the OPV (450 nm) or PERY (520 nm) chromophore with femtosecond pump−probe photoinduced absorption spectroscopy. Figure 3 shows an example of the transient traces that have been obtained. For each triad, k_{CS} and k_{CR} were extracted from the data by fitting a biexponential function. These data are collected in Table 1. For all three triads, charge separation is extremely fast ($k_{CS} = 2.2 \times 10^{11}$ to 1.6×10^{12} s^{-1}, Table 1). The charge recombination varies more strongly with the solvent and is in general slower ($k_{CR} = <8 \times 10^8$ to 2.6×10^{11} s^{-1}). We found that values obtained for k_{CS} (or k_{CR}) pertaining to the same solute−solvent combination were independent of the excitation wavelength (450 or 520 nm) used. This indicates that an ultrafast singlet energy transfer from the singlet excited state of OPV (2.52 eV) to the PERY moiety precedes the electron transfer, which therefore originates from PERY singlet excited state S_1. The strong quenching of the OPV fluorescence supports this conclusion. Therefore, the change in free energy for charge separation, $-\Delta G_0$, was determined relative to the energy level of the PERY S_1 (E_{00}) and the redox potentials of the donor (E_{ox}(D)) and the acceptor (E_{red}(A)) state using a continuum model:[7]

$$-\Delta G_0 = -e[E_{ox}(\mathrm{D}) - E_{red}(\mathrm{A})] + E_{00} + \frac{e^2}{4\pi\epsilon_0\epsilon_s R_{cc}} + \frac{e^2}{8\pi\epsilon_0}\left(\frac{1}{r^+} + \frac{1}{r^-}\right)\left(\frac{1}{\epsilon_{ref}} - \frac{1}{\epsilon_s}\right) \quad (1)$$

The radius of the OPV radical cation and the perylene bisimide anion are set to $r^+ = 5.05$ Å and $r^- = 4.71$ Å, respectively,[8] whereas the center-to-center chromophore distance (R_{cc}) was set at 14 Å for all three compounds.

A semilogarithmic plot of k_{CS} and k_{CR} versus $-\Delta G_0$ is given in Figure 4. The plot clearly shows that charge recombination (open symbols) takes place in the inverted region. The rates can be described using the nonadiabatic electron-transfer theory proposed by Jortner et al.:[9]

$$k_0 = \left(\frac{\pi}{\hbar^2\lambda_s k_B T}\right)^{1/2} V^2 \sum_{n=0}^{\infty} e^{-S}\frac{S^n}{n!} \exp\left(-\frac{(\Delta G_0 + \lambda_s + n\hbar\omega)^2}{4\lambda_s k_B T}\right) \quad (2)$$

In eq 2, V describes the electronic coupling and S ($= \lambda_i/\hbar\omega$) relates to the effective mode vibrational energy, whereas λ_i and λ_s are the internal and solvent reorganization energies, respectively. Taking $\hbar\omega = 0.186$ eV (1500 cm^{-1}) and $T = 298$ K, a satisfactory fit could be obtained for $\lambda_i = 0.25$ eV, $\lambda_s = 0.5$ eV, and $V = 6$ meV (Figure 4). This value of λ_s is in reasonable agreement with values calculated with the Born−Hush approximation for the more polar solvents.[10]

TABLE 1: Experimental Rate Constants (k) and Estimates for the Change in the Gibbs Free Energy (ΔG) and Activation Energy ($\Delta G^{\ddagger}$) for Charge Separation (CS) and Recombination (CR) in Different Solvents[a]

	solvent	$-\Delta G_{CS}$ (eV)	$\Delta G^{\ddagger}_{CS}$[b] (eV)	k_{CS} (s^{-1})	$k_{CS,calcd}$[c] (s^{-1})	$-\Delta G_{CR}$ (eV)	$\Delta G^{\ddagger}_{CR}$[b] (eV)	k_{CR} (s^{-1})	$k_{CR,calcd}$[d] (s^{-1})
1	$PhCH_3$	0.14	0.021	2.7×10^{11}	1.4×10^{10}	1.99	2.73	$<8 \times 10^{8}$	1.1×10^{8}
	$PhCH_3$[e]				4.9×10^{11}				5.7×10^{8}
	$CHCl_3$	0.55	0.016	2.2×10^{11}	4.5×10^{11}	1.58	0.212	2.1×10^{10}	6.4×10^{9}
	PhCl	0.61	0.006	2.6×10^{11}	5.2×10^{11}	1.52	0.204	1.0×10^{10}	1.1×10^{10}
	THF	0.69	0.019	3.9×10^{11}	5.7×10^{11}	1.44	0.057	3.4×10^{10}	2.1×10^{10}
	ODCB	0.76	0.003	4.6×10^{11}	5.8×10^{11}	1.37	0.078	1.8×10^{10}	3.5×10^{10}
	PhCN	0.88	0.004	2.5×10^{11}	5.8×10^{11}	1.25	0.016	5.5×10^{10}	7.9×10^{10}
2	$PhCH_3$	0.51	0.037	1.6×10^{12}	4.1×10^{11}	1.81	1.89	3.0×10^{9}	7.4×10^{9}
	$PhCH_3$[e]				4.1×10^{11}				3.9×10^{9}
	$CHCl_3$	0.91	0.007	1.5×10^{12}	6.0×10^{11}	1.40	0.128	6.6×10^{10}	2.8×10^{10}
	PhCl	0.98	0.020	1.0×10^{12}	6.6×10^{11}	1.34	0.120	7.5×10^{10}	4.3×10^{10}
	THF	1.06	0.002	1.5×10^{12}	7.9×10^{11}	1.26	0.022	8.9×10^{10}	7.5×10^{10}
	ODCB	1.13	0.022	1.1×10^{12}	9.1×10^{11}	1.19	0.033	4.4×10^{10}	1.1×10^{11}
	PhCN	1.25	0.015	1.3×10^{12}	1.0×10^{12}	1.07	0.001	9.3×10^{10}	2.2×10^{11}
3	$PhCH_3$	0.77	0.185	1.5×10^{12}	5.8×10^{11}	1.61	1.43	1.6×10^{10}	4.9×10^{9}
	$PhCH_3$[e]				1.1×10^{12}				2.5×10^{10}
	$CHCl_3$	1.18	0.054	1.0×10^{12}	9.9×10^{11}	1.20	0.060	1.2×10^{11}	1.1×10^{11}
	PhCl	1.24	0.085	8.7×10^{11}	1.0×10^{12}	1.14	0.053	6.4×10^{10}	1.5×10^{11}
	THF	1.32	0.033	1.0×10^{12}	1.0×10^{12}	1.06	0.002	2.6×10^{11}	2.3×10^{11}
	ODCB	1.39	0.082	9.0×10^{11}	9.7×10^{11}	0.99	0.006	7.9×10^{10}	3.1×10^{11}
	PhCN	1.51	0.064	5.8×10^{11}	7.3×10^{11}	0.87	0.004	1.9×10^{11}	4.5×10^{11}

[a] Calculated rate constants following eq 2. [b] Determined from the Marcus relation $\Delta G^{\ddagger} = (\Delta G_0 + \lambda)^2/4\lambda$, with $\lambda = \lambda_i + \lambda_s$, $\lambda_i = 0.25$ eV, and $\lambda_s = (e^2/4\pi\epsilon_0)(1/(2r^+) + 1/(2r^-) - (1/R_{cc}))(1/n^2 - 1/\epsilon_s)$.[10] [c] Calculated for both the PERY $S_1 \rightarrow$ CSS and PERY $S_1 \rightarrow$ CSS* pathways ($k_{CS,calcd} = k_{CSS} + k_{CSS*}$) using $\lambda_i = 0.25$ eV, $\lambda_s = 0.5$ eV, $V_{CSS} = 6$ meV, $V_{CSS*} = 8$ meV, $\hbar\omega = 0.186$ eV ($\omega = 1500$ cm^{-1}), and $T = 298$ K. [d] Calculated for CSS $\rightarrow$ S_1 using $\lambda_i = 0.25$ eV, $\lambda_s = 0.5$ eV, $V = 6$ meV, $\hbar\omega = 0.186$ eV, and $T = 298$ K. [e] Calculated using $\lambda_s = 0.1$ eV instead of 0.5 eV. (See the text).

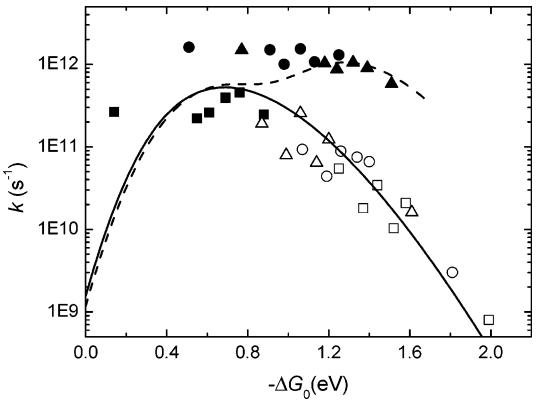

Figure 4. Rates for charge separation (solid markers) and recombination (open markers) versus $-\Delta G_0$ for **1** (squares), **2** (circles), and **3** (triangles). The solid line represents k calculated from eq 1. The dashed line represents the calculated k for a combination of charge separation to CSS and CSS*, taking into account a 0.6-eV lower driving force for the latter pathway. The data for charge separation in toluene (in parentheses) were not used in the fitting because the solvent reorganization energy λ_s deviates significantly from that in the other solvents (see text).

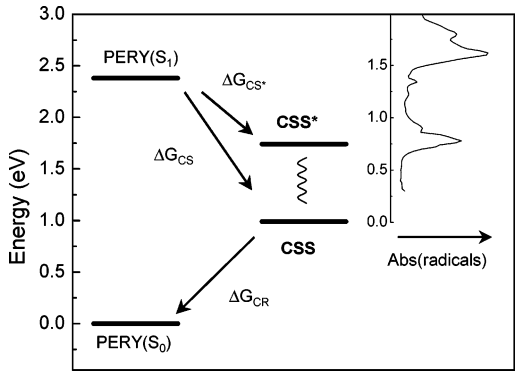

Figure 5. Energy diagram for charge separation from PERY S_1 to CSS and CSS*. The inset shows the absorption spectrum of OPV−$PERY^{-\bullet}$−$OPV^{+\bullet}$ relative to the energy level of CSS.

Turning now to the rates for charge separation (Figure 4, solid markers), it appears that the k_{CS} data of **1** fall on the same curve as used to describe the charge recombination. Charge separation for **1** is close to the "optimal region" ($-\Delta G_0 \approx \lambda$). For **2** and **3**, charge separation is more exergonic than for **1**, and the rates for charge separation are expected to be lower because inverted behavior applies. In contrast, the experimental charge separation in **2** and **3** is significantly faster than in **1** (Figure 4). Nevertheless, a small reduction of k_{CS} (more pronounced for **3**) with increasing $-\Delta G_0$ indicates behavior close to the inverted region.

A possible explanation for the high k_{CS} of **2** and **3** is that charge transfer produces an excited state of the charge-separated state (CSS*) rather than the ground state (CSS, Figure 5).[4c] The energy of CSS* can be inferred from the absorption spectrum of $OPV^{+\bullet}$, which exhibits a low-energy band with an onset at 0.6 eV (Figure 5).[11] Because $-\Delta G_0$ (to CSS) exceeds 0.6 eV in solvents with $\epsilon > 2.7$, charge transfer from the PERY S_1 state to CSS* is exergonic for **2** and **3**. We expect that nonradiative decay from CSS* to CSS is fast; therefore, we consider that charge recombination occurs only from CSS.

When $-\Delta G_0$ is corrected for the 0.6-eV difference between CSS and CCS*, the charge transfer will become less exergonic and is no longer expected to occur in the inverted region but rather in the optimal region. This rationalizes the moderate reduction of k_{CS} with increasing $-\Delta G_0$ and explains (in part) the high values of k_{CS} for **2** and **3**. By including the additional pathway to CSS* with a 0.6-eV lower driving force, the experimental data for k_{CS} of **2** and **3** are in fair agreement with values obtained from eq 2 when the same parameters are used as before and the electronic coupling between PERY S_1 and CSS* is set to $V = 8$ meV (i.e., slightly higher that between PERY S_1 and CSS ($V = 6$ meV)). For low values of $-\Delta G_0$, the rate constant does not change because the pathway to CSS* is endergonic. For larger values of $-\Delta G_0$, charge separation is a combination of both pathways. The fit supports the presence

of an additional charge-separation pathway to CSS* and reproduces the decrease of k_{CS} with increasing $-\Delta G_0$ for **2** and **3**.

The three experimental rate constants for the charge separation of **1**−**3** in toluene (indicated in Figure 4 with parenthesis) deviate from the calculated curve. This is primarily due to the fact that the solvent reorganization energy $\lambda_s = 0.5$ eV, used to construct the curve, does not apply to apolar solvents such as toluene. For toluene, the Born−Hush approximation gives $\lambda_s = 0.1$ eV. Using the same parameters but setting $\lambda_s = 0.1$ eV brings the calculated rate constants for toluene closer to the experimental values (Table 1). The deviation of the toluene data might also be explained by the notion that the microscopic polarity, and hence $-\Delta G_0$, is not accurately described by ϵ_s because of a substantial quadrupole moment of the solvent.[12]

Conclusions

The kinetics of photoinduced intramolecular charge separation and charge recombination in three homologous oligo(*p*-phenylene vinylene)-perylene bisimide-oligo(*p*-phenylene vinylene) arrays has been studied in solvents of different polarity. For the two molecules with the lowest reduction potentials, **2** and **3**, the rates for charge separation and charge recombination decrease with increasing change in the Gibbs free energy and hence represent an example of molecules in which charge separation and recombination occur close to or in the Marcus inverted region.

Experimental Section

All of the solvents and reagents were purchased from Merck and used as received. 1,6,7,12-Tetra(4-*tert*-butylphenoxy)perylene-3,4:9,10-tetracarboxylic acid bisanhydride was synthesized according to the literature.[13] NMR spectra were recorded at room temperature on a Bruker DRX 400 spectrometer. Matrix-assisted laser desorption ionization time-of-flight (MALDI-TOF) mass spectrometry was recorded on a Bruker Franzen Reflex III spectrometer (dithranol matrix). The solvents for spectroscopic studies were of spectroscopic grade and used as received. UV/vis spectra were measured on a Perkin-Elmer Lambda 40P, and the steady-state fluorescence spectra were measured on a Perkin-Elmer LS-50B spectrofluorometer.

***N,N′*-Di[(*E,E,E*)-4-[4-{4-(3,4,5-tridodecyloxystyryl)-2,5-bis[(*S*)-2-methylbutoxy]styryl}-2,5-bis[(*S*)-2-methylbutoxy]-styryl]phenyl]-1,6,7,12-tetra(4-*tert*-butylphenoxy)perylene-3,4:9,10-tetracarboxylic Acid Bisimide (1).** (*E,E,E*)-4-[4-{4-(3,4,5-Tridodecyloxystyryl)-2,5-bis[(*S*)-2-methylbutoxy]styryl}-2,5-bis[(*S*)-2-methylbutoxy]styryl]aniline[6] (120 mg, 0.095 mmol), 1,6,7,12-tetrakis(4-*tert*-butylphenoxy)-3,4:9,10-perylenetetracarboxylic dianhydride[13] (38 mg, 0.040 mmol), and zinc acetate (9 mg, 0.04 mmol) were mixed with 2 mL of quinoline. The reaction mixture was stirred under Ar for 16 h at 190 °C. After cooling to room temperature, it was added to a mixture of 1 mL of water and 10 mL of MeOH, and the precipitate was collected by filtration, washed with water and MeOH, and then dried in vacuum. The crude product was purified by silica gel column chromatography with CH_2Cl_2 as the eluent. After the solvent was evaporated, the product was precipitated from CH_2Cl_2 as a dark-purple powder by adding MeOH (60 mg, 43%); mp 302 °C; ^{1}H NMR (400 MHz, $CDCl_3$, 25 °C, TMS): $\delta = 8.26$ (s, 4H; $H_{perylene}$), 7.7−7.0 (m, 44H; Ar−H, vinylic H), 6.86 (d, $J = 8.8$ Hz, 8H; Ar−H), 6.74 (s, 4H; Ar−H), 4.02 (t, $J = 6.5$ Hz, 8H; $-OCH_2C_{11}H_{23}$), 3.97 (t, $J = 6.1$ Hz, 4H; $-OCH_2C_{11}H_{23}$), 3.81−3.95 (m, 16H; $-OCH_2-$), 2.1−1.2 (m, 180H), 1.1(m, 24H; $-CH_3$), 1.0 (m, 24H; $-CH_3$), 0.9 (t, $J = 6.1$ Hz, 18H; $-CH_3$); ^{13}C NMR (100 MHz, $CDCl_3$, 25 °C): $\delta = 163.61$, 156.13, 153.26, 152.84, 151.42, 151.18, 151.11, 151.00, 147.45, 138.63, 138.20, 133.97, 133.25, 133.14, 129.64, 128.74, 128.59, 127.91, 127.75, 127.44, 127.17, 126.84, 126.69, 126.41, 124.77, 122.82, 122.60, 120.77, 120.23, 119.79, 119.37, 110.97, 110.49, 109.93, 109.66, 105.15, 74.52, 74.47, 74.21, 74.07, 73.56, 69.12, 35.16, 35.09, 34.99, 34.36, 31.94, 31.92, 31.41, 30.36, 29.76, 29.74, 29.71, 29.70, 29.66, 29.47, 29.44, 29.39, 29.36, 26.40, 26.35, 26.13, 22.68, 16.86, 16.78, 14.10, 11.51, 11.47, 11.38; MALDI-TOF MS calculated for $C_{236}H_{326}N_2O_{22}$, 3540.4 *m/z*; found, 3542.8 $[M + H]^+$; UV/vis (CH_2Cl_2) $\lambda_{max}(\epsilon) = 581$ (62 800), 541 (40 200), 436 (151 000), 336 (54 600), 289 nm (72 600 mol^{-1} L cm^{-1}); fluorescence (MCH, 3.0×10^{-7} mol L^{-1}): $\lambda_{max} = 592$ nm.

***N,N′*-Di[(*E,E,E*)-4-[4-{4-(3,4,5-tridodecyloxystyryl)-2,5-bis[(*S*)-2-methylbutoxy]styryl}-2,5-bis[(*S*)-2-methylbutoxy]-styryl]phenyl]-1,6,7,12-tetrachloroperylene-3,4:9,10-tetracarboxylic Acid Bisimide (3).** The compound was synthesized according to the above procedure for **1**. Starting from (*E,E,E*)-4-[4-{4-(3,4,5-tridodecyloxystyryl)-2,5-bis[(*S*)-2-methylbutoxy]-styryl}-2,5-bis[(*S*)-2-methylbutoxy]styryl]aniline[6] (80 mg, 0.063 mmol), 1,6,7,12-tetrachloro-3,4:9,10-perylenetetracarboxylic dianhydride[14] (15 mg, 0.028 mmol), and zinc acetate (6 mg, 0.026 mmol), the product was isolated as a red powder (35 mg, 40%); mp 305 °C; ^{1}H NMR (400 MHz, $CDCl_3$, 25°C, TMS): $\delta = 8.51$ (s, 4H; $H_{perylene}$), 7.5−6.8 (m, 28H; Ar−H, vinylic H), 6.58(s, 4H; Ar−H), 3.95 (m, 12H; $-OCH_2C_{11}H_{23}$), 3.79 (broad, 16H, $-OCH_2-$), 2.1−1.2 (m, 144H), 1.1(m, 24H; $-CH_3$), 1.0 (m, 24H; $-CH_3$), 0.9 (t, $J = 6.1$ Hz, 18H; $-CH_3$); ^{13}C NMR (100 MHz, $CDCl_3$, 25 °C): $\delta = 161.82$, 156.13, 153.14, 150.92, 150.76, 138.13, 134.54, 132.90, 128.99, 128.51, 126.84, 126.69, 126.33, 125.00, 123.47, 122.89, 122.31, 122.21, 109.79, 108.95, 105.01, 74.44, 74.01, 74.21, 73.84, 73.55, 69.07, 35.21, 35.13, 35.03, 34.93, 31.94, 30.41, 29.78, 29.74, 29.70, 29.47, 29.49, 29.38, 26.48, 26.42, 26.16, 22.69, 16.97, 16.91, 14.11, 11.58, 11.55, 11.51, 11.46; MALDI-TOF MS calculated for $C_{196}H_{274}Cl_4N_2O_{18}$, 3083.9 *m/z*; found, 3083.1 $[M]^+$; UV/vis (CH_2Cl_2): $\lambda_{max}(\epsilon) = 521$ (67 000), 433 (144 000), 335 nm (54 800 mol^{-1} L cm^{-1}).

Electrochemical Measurements. Cyclic voltammetry was performed with an EG&G PAR 273 potentiostat in a three-electrode single-compartment cell using dichloromethane as the solvent. Working electrode: platinum disk; counter electrode: platinum wire; reference electrode: Ag/AgCl. All potentials were internally referenced to the Fc/Fc^+ couple. The solutions were purged with argon gas prior to use. The supporting electrolyte was 0.1 mol L^{-1} tetrabutylammonium hexafluorophosphate (Fluka), which was recrystallized twice from ethanol/water and dried in a high vacuum.

Pump−Probe Experiments. The femtosecond laser system used for pump−probe experiments consisted of an amplified Ti/sapphire laser (Spectra Physics Hurricane). The single pulses from a cw mode-locked Ti/sapphire laser were amplified by a Nd:YLF laser using chirped-pulse amplification, providing 150-fs pulses at 800 nm with an energy of 750 μJ and a repetition rate of 1 kHz. The pump pulses (450 or 520 nm) were created via optical parametric amplification (OPA) of the 800-nm pulse by a BBO crystal into infrared pulses, which were then two times frequency doubled via BBO crystals. The pump beam was focused to a spot size of about 1 mm^2 with an excitation pulse energy of ~1 μJ. The probe beam (1450 nm) was generated in a separate optical parametric amplification setup. For the probe pulses, an RG 850-nm cutoff filter was used to avoid contributions of the residual probe light (800 nm) from

the OPA. The probe beam was reduced in intensity compared to that of the pump beam and polarized at the magic angle (54.7°) with respect to the pump beam polarization to cancel out orientation effects in the measured dynamics. The cross correlation of pump and probe pulses was determined by measuring the optical Kerr effect in pure heptane using the same sample cell as in the pump−probe experiments. The pump laser pulse induces birefringence because the refractive index contains an intensity-dependent term and becomes anisotropic under polarized illumination.[15] The cross correlation has an approximately Gaussian shape with 0.5-ps fwhm. In principle, rates for charge separation should be obtained by deconvoluting the measured signal with the cross correlation. However, numerical analysis indicates that for rates <2 ps^{-1} deconvolution results in only a negligible correction to the rate obtained by directly fitting an exponential function. The temporal evolution of the differential transmission was recorded using an InGaAs detector by a standard lock-in technique at 500 Hz.

Acknowledgment. We thank P. Jonkheijm and E. Peeters for synthetic contributions. This work has been supported by CW-NWO in the PIONIER program and by the DFG (grant Wu 317/5). The research of S.C.J.M. has been made possible by a fellowship from the Royal Dutch Academy of Arts and Sciences.

Supporting Information Available: Cyclic voltammograms of **1**−**3**. This material is available free of charge via the Internet at http://pubs.acs.org.

References and Notes

(1) (a) *Advances in Chemical Physics*; Jortner, J., Bixon, M., Ed.; Wiley-Interscience: 1999; Vols. 106 and 107. (b) *Electron Transfer in Chemistry*; Balzani, V., Ed.; Wiley-VCH: Weinheim, Germany, 2001; Vols. 1−5.

(2) (a) Marcus, R. A. *J. Chem. Phys.* **1965**, *43*, 679. (b) Marcus, R. A.; Sutin, N. *Biochim. Biophys. Acta* **1985**, *811*, 265. (c) Marcus, R. A. *Rev. Mod. Phys.* **1993**, *65*, 599.

(3) (a) Miller, J. R.; Calcaterra, L. T.; Closs, G. L. *J. Am. Chem. Soc.* **1984**, *106*, 3047. (b) Closs, G. L.; Miller, J. R. *Science* **1988**, *240*, 440.

(4) (a) Closs, G. L.; Calcaterra, L. T.; Green, N. J.; Penfield, K. W.; Miller, J. R. *J. Phys. Chem.* **1986**, *90*, 3673. (b) Asahi, T.; Ohkohchi, M.; Matsusaka, R.; Mataga, N.; Zhang, R. P.; Osuka, A.; Maruyama, K. *J. Am. Chem. Soc.* **1993**, *115*, 5665. (c) Heitele, H.; Pöllinger, F.; Häberle, T.; Michel-Beyerle, M. E.; Staab, H. A. *J. Phys. Chem.* **1994**, *98*, 7402. (d) Macpherson, A. N.; Liddell, P. A.; Lin, S.; Noss, L.; Seely, G. R.; DeGraziano, J. M.; Moore, A. L.; Moore, T. A.; Gust, D. *J. Am. Chem. Soc.* **1995**, *117*, 7202. (e) Häberle, T.; Hirsch, J.; Pöllinger, F.; Heitele, H.; Michel-Beyerle, M. E.; Anders, C.; Döhling, A.; Krieger, C.; Rückemann, A.; Staab, H. A. *J. Phys. Chem.* **1996**, *100*, 18269. (f) Osuka, A.; Noya, G.; Taniguchi, S.; Okada, T.; Nishimura, Y.; Yamazaki, I.; Mataga, N. *Chem.*−*Eur. J.* **2000**, *6*, 33.

(5) Mataga, N.; Chosrowjan, H.; Taniguchi, S.; Shibata, Y.; Yoshida, N.; Osuka, A.; Kikuzawa, T.; Okada, T. *J. Phys. Chem. A* **2002**, *106*, 12191.

(6) Peeters, E.; Van Hal, P. A.; Meskers, S. C. J.; Janssen, R. A. J.; Meijer, E. W. *Chem.*−*Eur. J.* **2002**, *8*, 4470.

(7) Weller, A. *Z. Phys. Chem.* **1982**, *133*, 93.

(8) Neuteboom, E. E.; Meskers, S. C. J.; Van Hal, P. A.; van Duren, J. K. J.; Meijer, E. W.; Janssen, R. A. J.; Dupin, H.; Pourtois, G.; Cornil, J.; Lazzaroni, R.; Brédas, J.-L.; Beljonne, D. *J. Am. Chem. Soc.* **2003**, *125*, 8625.

(9) (a) Kestner, N. R.; Logan, J.; Jortner, J. *J. Phys. Chem.* **1974**, *78*, 2148. (b) Ulstrup, J.; Jortner, J. *J. Chem. Phys.* **1975**, *63*, 4358.

(10) Hush, N. S. *Trans. Faraday Soc.* **1961**, *57*, 557.

(11) Van Hal, P. A.; Beckers, E. H. A.; Peeters, E.; Apperloo, J. J.; Janssen, R. A. J. *Chem. Phys. Lett.* **2000**, *328*, 403.

(12) Würthner, F.; Yao, S.; Debaerdemaeker, T.; Wortmann, R. *J. Am. Chem. Soc.* **2002**, *124*, 9431.

(13) (a) Seybold, G.; Wagenblast, G. *Dyes Pigm.* **1989**, *11*, 303. (b) Dotcheva, D.; Klapper, M.; Müllen, K. *Macromol. Chem. Phys.* **1994**, *195*, 1905. (c) Würthner, F.; Thalacker, C.; Sautter, A.; Schärtl, W.; Ibach, W.; Hollricher, O. *Chem.*−*Eur. J.* **2000**, *6*, 3871.

(14) Sadrai, M.; Hadel, L.; Sauers, R. R.; Husain, S.; Krogh-Jespersen, K.; Westbrook, J. D.; Bird, G. R. *J. Phys. Chem.* **1992**, *96*, 7988.

(15) Akhmanov, S. A.; Nikitin, S. Y. *Physical Optics*; Clarendon Press: Oxford, England, 1997.